PERGAMON

International Journal of Solids and Structures 36 (1999) 5277–5300

INTERNATIONAL JOURNAL OF SOLIDS and STRUCTURES

www.elsevier.com/locate/ijsolstr

Axisymmetric shells and plates on tensionless elastic foundations

T. Hong, J.G. Teng*, Y.F. Luo

Department of Civil and Structural Engineering, The Hong Kong Polytechnic University, Hong Kong, China

Received 18 December 1997; in revised form 14 July 1998; accepted 24 July 1998

Abstract

This paper first describes a finite element method for the large deflection analysis of axisymmetric shells and plates on a nonlinear tensionless elastic foundation. Through the use of discrete data points, any form of nonlinear elastic foundation behaviour can be easily modelled. The analysis is then validated by comparison with existing results for circular plates and beams as the only existing results for shells on tensionless foundations are found to be in error. Following this verification, the analysis is applied to investigate the behaviour of shallow spherical shells subject to a central concentrated load on tensionless linear elastic foundations. A number of insightful conclusions regarding the behaviour of such structure-foundation systems are drawn. The numerical results for shells are believed to be the first correct results, which may be useful in benchmarking results from other sources in the future.

1. Introduction

Shells and plates on elastic foundations are found in many practical applications. A number of different foundation models have been proposed in the past, with the simplest being the Winkler (1867) model. In a Winkler foundation model, the foundation reactions are assumed to be a linear function of the displacements of the supported structure. Consequently, the foundation is assumed to react to both compression and tension in the same manner and to be always in contact with the structure. Structures on Winkler foundations have been extensively studied by many investigators (Vlasov and Leontev, 1966), particularly concerning their linear elastic behaviour. Some work also exists on shells on nonlinear foundations which react in the same manner to both tension and compression (Luo and Teng, 1998).

The simple idealization of foundation behaviour in a Winkler model is not valid for many real supporting media, the commonest of which is the soil which is practically incapable of sustaining

* Corresponding author. Tel.: 00 852 2766 6073; fax: 00 852 2334 6389; e-mail: cejgt@polyu.edu.hk

0020-7683/99/$ - see front matter
PII: S0020-7683(98)00228-5

any tensile forces. The Winkler hypothesis was motivated more by the desire for mathematical simplicity than physical reality. For structures on soils and other supporting media capable of resisting compressive stresses only, the tensionless foundation model should be used for accurate modelling if the possibility exists for tensile stresses to develop at the interface between the structure and the foundation.

Analysis of a structure on a tensionless elastic foundation is difficult as separation can occur between the structure and the foundation, and in general, the region of contact is not known a priori. Even for a linear elastic structure on a tensionless elastic foundation which reacts linearly to compression (referred to as a linear tensionless elastic foundation or simply linear tensionless foundation later), the analysis needs to be performed iteratively. As a result, only a small number of studies on structures on linear tensionless elastic foundations have been published, and even less is known about structures on nonlinear tensionless foundations.

Tsai and Westmann (1967) considered a linear tensionless foundation and presented an iterative scheme that gives the solution for a structure on a tensionless foundation from that for a structure on a Winkler foundation. Weitsman (1970) studied the static behaviour of a beam resting on a tensionless elastic foundation subjected to a concentrated load and to a uniformly distributed load. More recently, beams on a tensionless foundation under a moving load was studied by Lin and Adams (1988).

Some of the early attempts to analyze plates supported by a linear tensionless elastic foundation were made by Weitsman (1970), but the results were later found to be slightly in error. Weitsman (1972) gave some corrections to his earlier work (Weitsman, 1970). Svec (1974) employed the finite element method to investigate the problem of plates of various shapes on tensionless foundations. Gladwell (1976) considered a variety of plane, frictionless, unbonded contact problems and provided approximate solutions in terms of Chebyshev polynomials. The problem of transversely loaded circular plates resting on bimodulus and tensionless foundations was addressed by Kamiya (1977) using an approximate approach. The equilibrium configuration of a free rectangular plate supported on a tensionless elastic foundation was studied by Villaggio (1983) and Li and Dempsey (1988). More recently, Celep (1988a, b) addressed the behaviour of circular and rectangular plates on tensionless elastic foundations under eccentric loading. A large deformation analysis of circular plates on a tensionless elastic foundation has been performed by Khathlan (1994). A limited amount of work also exists on elastic-plastic circular plates on tensionless foundations (Sokol-Supel, 1989) and rectangular plates on tensionless elastic-plastic foundations (Lewandowski and Switka, 1991).

Surprisingly little published information has been found on the analysis and behaviour of shells on tensionless foundations. The only study found on shells is due to Ghosh and Paliwal (1993) which describes a small deflection analysis for a shallow spherical shell on a tensionless foundation under a central concentrated load. The accuracy of their results was not checked as there were no previous results. No study on the large deflection behaviour of shells on tensionless foundations has been found.

This paper will first describe a finite element method for the large deflection analysis of axisymmetric shells and plates on a nonlinear tensionless elastic foundation. This work represents a further development of the analysis described in Luo and Teng (1998) which deals with the non-symmetric buckling analysis of shells of revolution on nonlinear elastic foundations which react in the same manner to both tension and compression. Through the use of discrete data points as

was done in Luo and Teng (1998), any form of nonlinear elastic foundation behaviour can be easily modelled. The analysis will then be validated by comparison with existing results for circular plates and beams as the only set of results for shells on tensionless foundations are found to be in error. Following this verification, the analysis will be applied to investigate the behaviour of shallow spherical shells subject to a central concentrated load on tensionless linear elastic foundations. A final example illustrates the capability of the analysis in dealing with nonlinear tensionless foundations.

2. Finite element analysis

2.1. The doubly-curved axisymmetric shell element

The doubly-curved isoparametric axisymmetric shell element used in the finite element formulation is shown in Fig. 1. The element geometry is defined in cylindrical coordinates by the radius R, the axial coordinate Z and the element meridional curvature $\mathrm{d}\varphi/\mathrm{d}s$ at the nodal points. The geometry is then interpolated between the nodes using cubic Hermitian functions. The nodal displacements are defined by u_i, $(\mathrm{d}u/\mathrm{d}s)_i$, v_i, $(\mathrm{d}v/\mathrm{d}s)_i$, w_i and $(\mathrm{d}w/\mathrm{d}s)_i$ in the global coordinate system at each ring node at the end of the element. The displacements within the element, expressed in the global coordinate system, u, v and w (Fig. 1) are interpolated between the nodal points in terms of the nodal values also using cubic Hermitian functions. The global displacements u, v and w at any point are related to the local displacements $\bar{u}$, $\bar{v}$ and $\bar{w}$ in the curvilinear coordinates by a transformation matrix $[T]$ (Teng and Rotter, 1989a).

2.2. Nonlinear finite element equations

The total Lagrangian approach is adopted in which all the quantities are referred to the undeformed configuration. The application of the principle of virtual displacements leads to a set of nonlinear equations for the finite element model of a given structure which may be represented by:

$$\{\mathbf{\Phi}(\boldsymbol{\delta})\} = \{\mathbf{F}\} + \{\mathbf{F}_s\} - \sum_{i=1}^{N} \int [B]^{\mathrm{T}} \{\mathbf{\Sigma}\}\, \mathrm{d}V = 0 \tag{1}$$

in which $\{\boldsymbol{\delta}\}$ is the vector of nodal displacement variables, $\{\mathbf{F}\}$ is the vector of equivalent nodal forces due to body forces and surface tractions, $\{\mathbf{F}_s\}$ is the vector of equivalent nodal forces due to the foundation reactions, N is the number of elements employed, $[B]$ is the incremental strain-displacement matrix based on the nonlinear shell theory of Rotter and Jumikis (1988) for shells of revolution which is a special case of the general nonlinear shell theory described in Teng and Hong (1997), $\{\mathbf{\Sigma}\}$ is the vector of stress resultants and $\{\mathbf{\Phi}(\boldsymbol{\delta})\}$ represents a vector of nodal residual forces. For each iteration, the nodal displacement increments for the structure $\{\mathbf{\Delta}\boldsymbol{\delta}\}$ are obtained by solving the linearised system of equations

$$\{\mathbf{\Phi}(\boldsymbol{\delta})\} = [K_{\mathrm{T}}]\{\mathbf{\Delta}\boldsymbol{\delta}\} \tag{2}$$

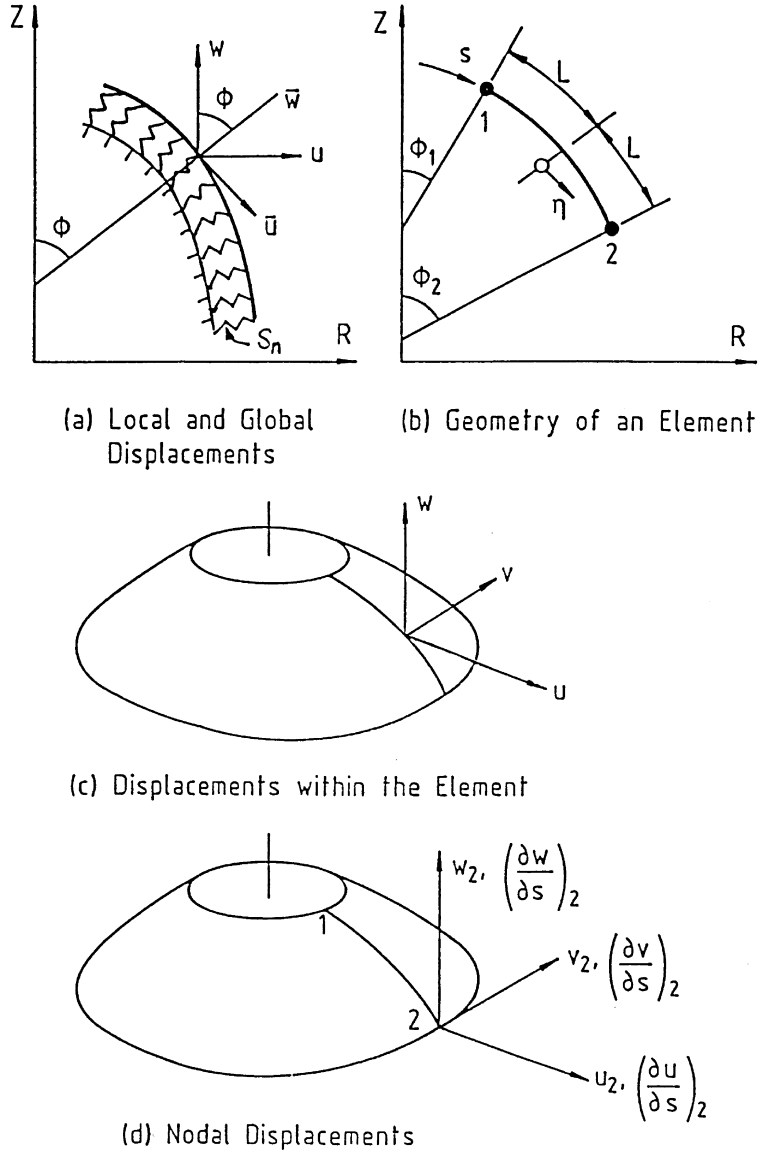

Fig. 1. Geometry and displacements of an element: (a) local and global displacements; (b) geometry of an element; (c) displacements within an element; (d) nodal displacements.

where $[K_T]$ is termed the global tangent stiffness matrix. The tangent stiffness matrix for each element is given by

$$[K_T]_e = [K]_e + [K_\sigma]_e + [K_s]_e \tag{3}$$

where $[K]_e$ is the stiffness matrix including the effect of changes in geometry, $[K_\sigma]_e$ accounts for the effect of internal stresses and $[K_s]_e$ is the element tangent stiffness matrix of the elastic foundation.

The element tangent stiffness matrices are condensed to reduce the inter-element continuity as described by Teng and Rotter (1989a). The global tangent stiffness matrix $[K_T]$ may then be found by assembling the condensed element tangent stiffness matrices.

2.3. A nonlinear tensionless elastic foundation model

The nonlinear tensionless foundation model to be described here is of the Winkler type and may be viewed as nonlinear springs (Figs 1 and 2). Although Fig. 1 shows only distributed springs normal to the shell surface, distributed springs over the whole or part of the shell surface in the three directions of the local coordinate system are all considered. The reaction-displacement curve of the tensionless foundation is represented by a number of discrete data points as shown in Fig. 2. These discrete points may be obtained from tests, or from a theoretical study. For simplicity of description here, negative displacements in the local coordinates are assumed to cause compression in the foundation, but the opposite case can also be handled easily in the formulation. The foundation reaction pressures are assumed to be positive when acting in the negative directions of local coordinates.

Let r be the reaction pressure of the foundation (in either of the three directions), and $\bar{\delta}$ be the corresponding displacement at any point of the shell surface, then, if $\bar{\delta}_i \geqslant 0$, $r_i = 0$ (Fig. 2). If the displacement is negative, a linear interpolation is used to find the foundation reaction for a given value of the displacement between two discrete data points. At any stage of the loading when the displacement is $\bar{\delta}_k$ which is between $\bar{\delta}_{i-1}$ and $\bar{\delta}_i$, the corresponding spring reaction pressure is evaluated as

$$r_k = r_{i-1} + s(\bar{\delta}_i - \bar{\delta}_{i-1}) \tag{4}$$

where the tangent stiffness of the spring is given by

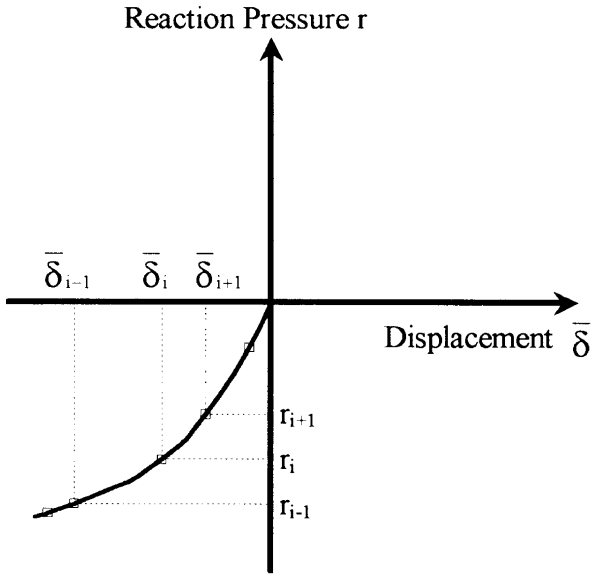

Fig. 2. Foundation reaction pressure-displacement relationship.

$$s = \frac{\mathrm{d}r}{\mathrm{d}\bar{\delta}} = \frac{r_i - r_{i-1}}{\bar{\delta}_i - \bar{\delta}_{i-1}} \tag{5}$$

The secant stiffness of the spring resistance is evaluated as

$$s_{\mathrm{b}} = \frac{r_k}{\bar{\delta}_k} \tag{6}$$

The vector of spring reaction pressure is related to the vector of displacements through

$$\{\mathbf{r}\} = \begin{Bmatrix} r_\phi \\ r_\theta \\ r_{\mathrm{n}} \end{Bmatrix} = \begin{bmatrix} s_{\mathrm{b}\phi} & 0 & 0 \\ 0 & s_{\mathrm{b}\theta} & 0 \\ 0 & 0 & s_{\mathrm{bn}} \end{bmatrix} \begin{Bmatrix} \bar{u} \\ \bar{v} \\ \bar{w} \end{Bmatrix}$$

$$= [\overline{K_{\mathrm{sb}}}]\{\bar{\boldsymbol{\delta}}\} = [\overline{K_{\mathrm{sb}}}][T]\{\boldsymbol{\delta}\} = [\overline{K_{\mathrm{sb}}}][T][N]\{\boldsymbol{\delta}^{\mathrm{e}}\} \tag{7}$$

where $s_{\mathrm{b}\phi}$, $s_{\mathrm{b}\theta}$ and s_{bn} are the secant stiffness of the springs in the meridional, circumferential and normal directions, respectively, $\{\boldsymbol{\delta}\}$ is the vector of displacements at any point on the shell reference surface in the global coordinate system, $\{\boldsymbol{\delta}^{\mathrm{e}}\}$ is the element nodal displacement vector in global coordinates, $[N]$ is a matrix of shape functions and $[T]$ a matrix transforming quantities in global coordinates to local coordinates (Teng and Rotter, 1989a). The incremental relation between the vector of spring reaction pressures and the vector of displacements is given by

$$\mathrm{d}\{\mathbf{r}\} = \begin{Bmatrix} \mathrm{d}r_\phi \\ \mathrm{d}r_\theta \\ \mathrm{d}r_{\mathrm{n}} \end{Bmatrix} = \begin{bmatrix} s_\phi & 0 & 0 \\ 0 & s_\theta & 0 \\ 0 & 0 & s_{\mathrm{n}} \end{bmatrix} \begin{Bmatrix} \mathrm{d}\bar{u} \\ \mathrm{d}\bar{v} \\ \mathrm{d}\bar{w} \end{Bmatrix}$$

$$= [\overline{K_{\mathrm{s}}}]\,\mathrm{d}\{\bar{\boldsymbol{\delta}}\} = [\overline{K_{\mathrm{s}}}][T]\,\mathrm{d}\{\boldsymbol{\delta}\} = [\overline{K_{\mathrm{s}}}][T][N]\,\mathrm{d}\{\boldsymbol{\delta}^{\mathrm{e}}\} \tag{8}$$

in which s_ϕ, s_θ and s_{n} are the tangent stiffness of the springs in the meridional, circumferential and normal directions, respectively. The vector of element nodal equivalent forces $\{\mathbf{F_s}\}_{\mathrm{e}}$ due to the spring reaction pressures is given by

$$\{\mathbf{F_s}\}_{\mathrm{e}} = -\int_A [N]^T[T]^T\{\mathbf{r}\}\,\mathrm{d}A \tag{9}$$

Consequently, the element tangent stiffness matrix of the springs in the global coordinates is given by

$$[K_{\mathrm{s}}]_{\mathrm{e}} = -\frac{\mathrm{d}\{\mathbf{F_s}\}_{\mathrm{e}}}{\mathrm{d}\{\boldsymbol{\delta}^{\mathrm{e}}\}} = \int_A [N]^T[T]^T\frac{\mathrm{d}\{\mathbf{r}\}}{\mathrm{d}\{\boldsymbol{\delta}^{\mathrm{e}}\}}\mathrm{d}A$$

$$= \int_A [N]^T[T]^T[\overline{K_{\mathrm{s}}}][T][N]\,\mathrm{d}A \tag{10}$$

3. Finite element implementation and results

The tensionless elastic foundation model proposed here has been coded into the NEPAS program (Teng and Rotter, 1989a, 1989b; Teng and Luo, 1997; Luo and Teng, 1998) for the nonlinear

and buckling analysis of shells of revolution. Some numerical examples are presented below to demonstrate the validity and capability of the tensionless foundation model as well as the finite element formulation. In addition, the behaviour of shallow spherical shells will be investigated in detail using the finite element program.

Apart from the one example at the end of the paper, all results described in the paper relate to a linear tensionless elastic foundation represented as a special case of the nonlinear tensionless foundation model of Fig. 2 and reacting only to displacements normal to the shell surface. As the boundary between a contact zone and a separation zone generally lies between the two end nodes of an element, its position is found by a simple linear interpolation of the normal displacements. While the use of the element shape function leads to more accurate results, this simpler approach leads to results of sufficiently high accuracy. It should also be noted that the vertical deflection w is taken to be positive when it is upward.

4. Numerical verification

4.1. Beams on tensionless foundations

Figure 3a shows a long beam of uniform section size subjected to a self weight q per unit length and a concentrated downward load P on a tensionless elastic foundation studied by Weitsman (1970). The behaviour of the beam was described by Weitsman using dimensionless lengths of the contact zone and separation zone ξ_0 and ξ_1 and the dimensionless load Q^*. These dimensionless quantities are defined as

$$\xi_0 = \beta X_0, \quad \xi_1 = \beta X_1, \quad Q^* = \beta \frac{P}{q} \tag{11}$$

where X_0 is the half length of the contact zone under the load P and X_1 is the distance between the load and the point where the beam comes into contact with the foundation again after separation (Fig. 3a). The parameter β is defined by $\beta^4 = k/(4EI)$ where k is the foundation stiffness and EI is the bending rigidity of the beam. The relationships between the dimensionless lengths ξ_0 and $(\xi_1 - \xi_0)$ against the dimensionless load Q^* are plotted in Fig. 3b and c, which show that the present results are in close agreement with those of Weitsman (1970).

4.2. Circular plates on a tensionless elastic foundation

The behaviour of circular plates on tensionless foundations has recently been studied by Khathlan (1994) using both the small deflection theory and the large deflection theory. As shown in Fig. 4, the plate has a radius R, a thickness t, and a flexural rigidity D. The Young's modulus of the plate material is E, and the Poisson's ratio $\nu = 0.3$. The circular plate is subject to a downward central load P. The results are plotted in a dimensionless manner using the dimensionless foundation stiffness $K^* = kR^4/D$, in which k is the foundation stiffness, and the dimensionless load $P^* = P/(ktR^2)$, in which P is the central downward load and the bending rigidity $D = Et^3/[12(1-\nu^2)]$.

Figure 5 shows comparisons between Khathlan's (1994) and the present results for various

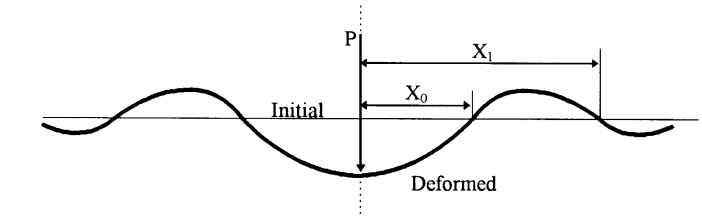

(a) Schematic of deformed shape

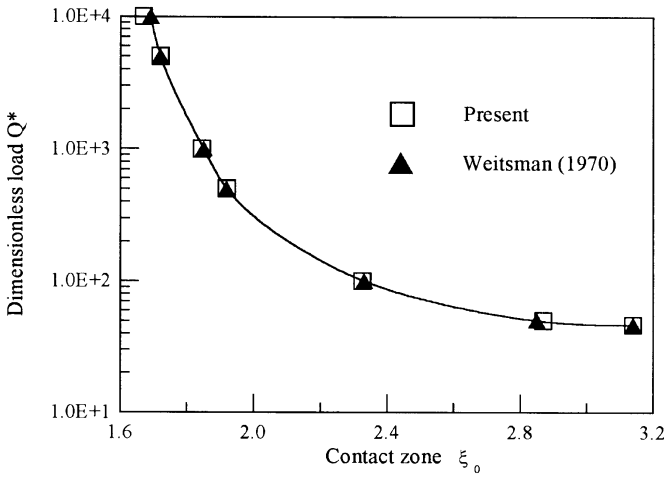

(b) Effect of load level on contact zone

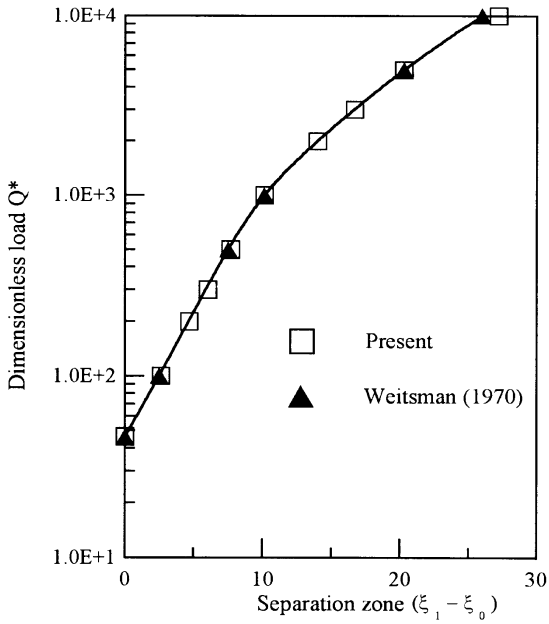

(c) Effect of load level on separation zone

Fig. 3. Beam on tensionless foundation: (a) schematic of deformed shape; (b) effect of load level on contact zone; (c) effect of load level on separation zone.

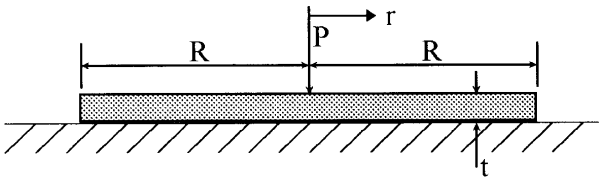

Fig. 4. Circular plate on tensionless foundation.

parameters of interest. These comparisons show a very close match between the two sets of results, confirming the accuracy of the present analysis. typical radial variations of the displacements are plotted in Fig. 5a, which shows the uplighting phenomenon of the plate. A significant difference is found between the predictions from the small deflection theory and those of the large deflection theory. The use of a large deflection theory leads to a stiffer structure-foundation system (Fig. 5a). The radius of contact R_c (i.e. the radius of the outer edge of the central contact zone) increases with the applied load based on the large deflection analysis, but is independent of the load level according to the small deflection analysis (Fig. 5b). For an accurate analysis of such plates with relatively large deflections (around $w/t > 0.5$ at the plate centre), the use of a large deflection analysis is essential. The variations of displacements with loads at the plate centre and at the plate edge predicted by large deflection analyses are shown in Fig. 5c and d, respectively.

4.3. A shallow spherical shell on a tensionless foundation

In many practical applications, thin shells are in contact with soils or other solids. As a result, many studies have been carried out on the analysis and behaviour of shells on elastic foundations. However, little information currently exists on the behaviour of shells on tensionless elastic foundations. Ghosh and Paliwal (1993) appear to have presented the first and only study on the behaviour of a shallow spherical shell resting on a tensionless foundation subject to a central concentrated load using the small deflection theory. The accuracy of their results was not verified due to the lack of previous results. It is therefore important to obtain more information for shells on tensionless foundations both for a better understanding of their structural behaviour, and to provide an independent check of the results of Ghosh and Paliwal (1993).

Figure 6 shows the geometry of a shallow spherical shell of the inverted dome type (referred to as an inverted spherical cap later) defined by the radius R, the shell depth H and the shell thickness t. The radius of curvature of the shell R_0 is related to R and H, so only two of these three parameters need to be specified. The spherical shell considered by Ghosh and Paliwal (1993) (Fig. 6) has the following material and geometric properties: $E = 2.1 \times 10^{10}$ kg m^{-2}, $v = 0.3$, $R_0 = 10$ m, $R = 2$ m, $t = 8$ mm. The foundation stiffness $k = 1.6 \times 10^4$ kg m^{-3}. Three cases of edge conditions were considered: clamped edge (C), simply supported edge (S) and free edge (F). This shell was also investigated by the present analysis. Figure 7 shows a comparison between the load deflection curves from Ghosh and Paliwal and those from the present analysis. It is clear that these two sets of results do not match. These differences have been carefully considered with the conclusion that the results of Ghosh and Paliwal (1993) are in error as the present analysis produces results in agreement with others for beams and circular plates as shown above.

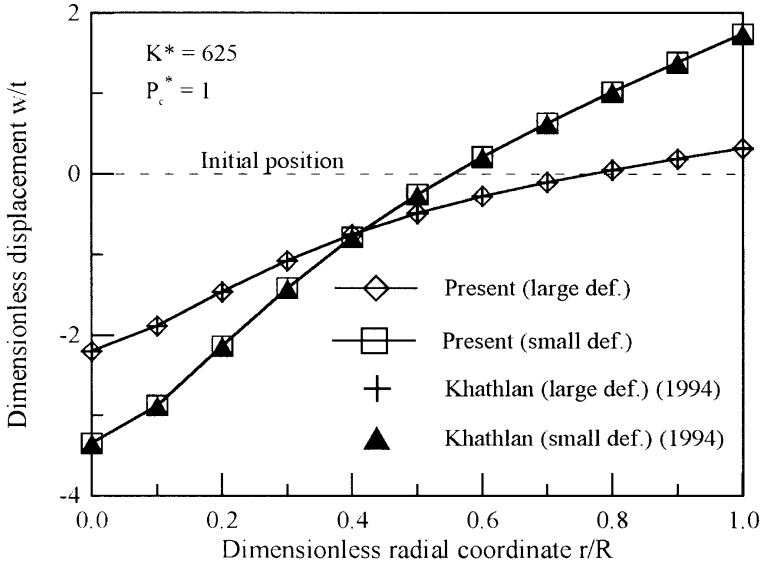

(a) Radial variations of displacement from small and large deflection analysis

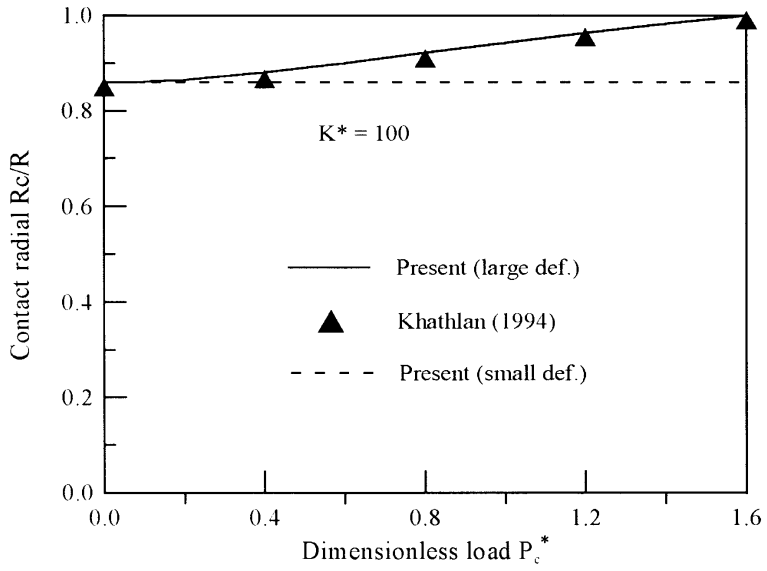

(b) Relation between radius of contact and applied load

Fig. 5. Response of a circular plate under a point load on tensionless foundation: (a) radial variations of displacement from small and large deflection analysis; (b) relation between radius of contact and applied load; (c) plate central displacement against load from large deflection analysis; (d) plate edge displacement against load from large deflection analysis.

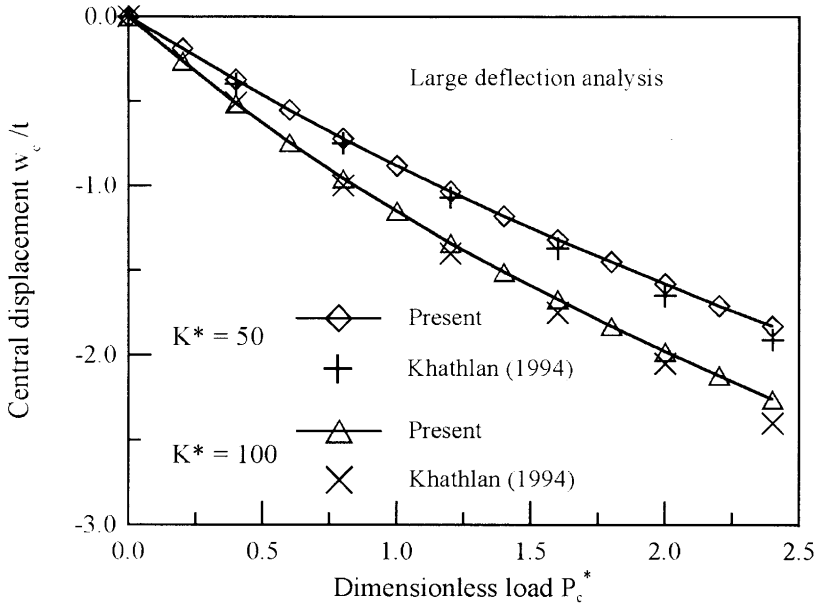

(c) Plate central displacement against load from large deflection analysis

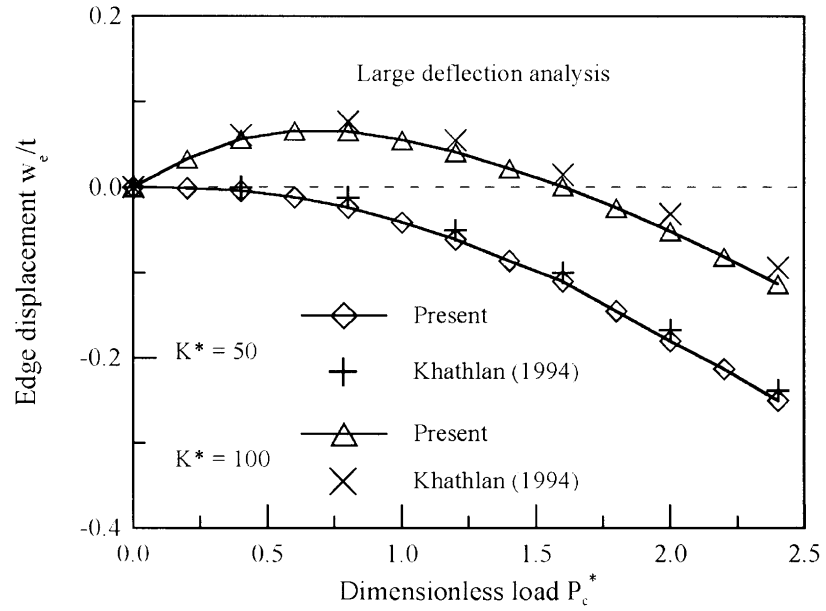

(d) Plate edge displacement against load from large deflection analysis

Fig. 5 (*continued*).

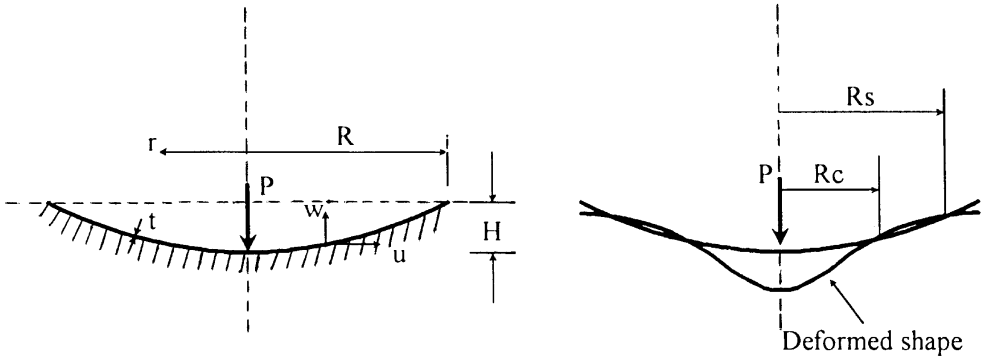

Fig. 6. Shallow spherical shell on tensionless foundation.

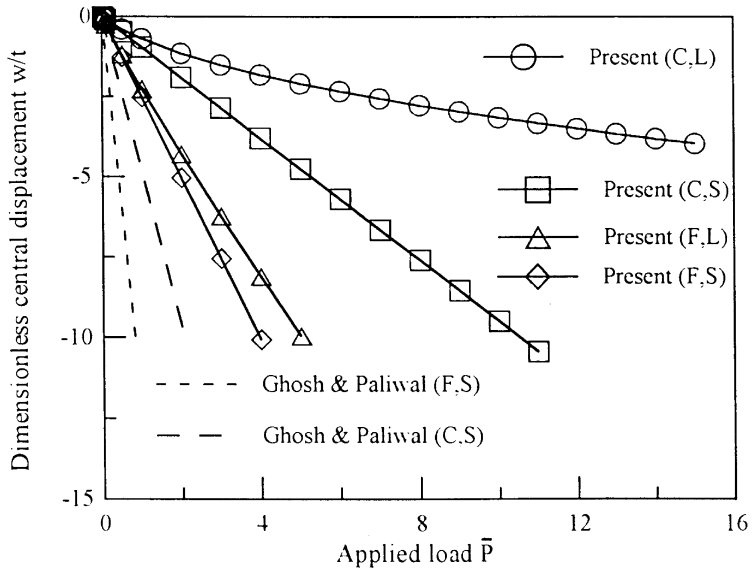

$\bar{P}$ = P / (2500kg); C = Clamped edge, F = Free edge
L = Large deflection analysis, S = Small deflection analysis

Fig. 7. Comparison for Ghosh and Paliwal's shallow spherical shell.

5. Inverted spherical caps on tensionless foundations

5.1. General

As the existing results of Ghosh and Paliwal (1993) are in error, a numerical parametric study was carried out in this study for inverted spherical caps without edge support on tensionless linear elastic foundations which react only to displacements normal to the shell surface. Apart from other

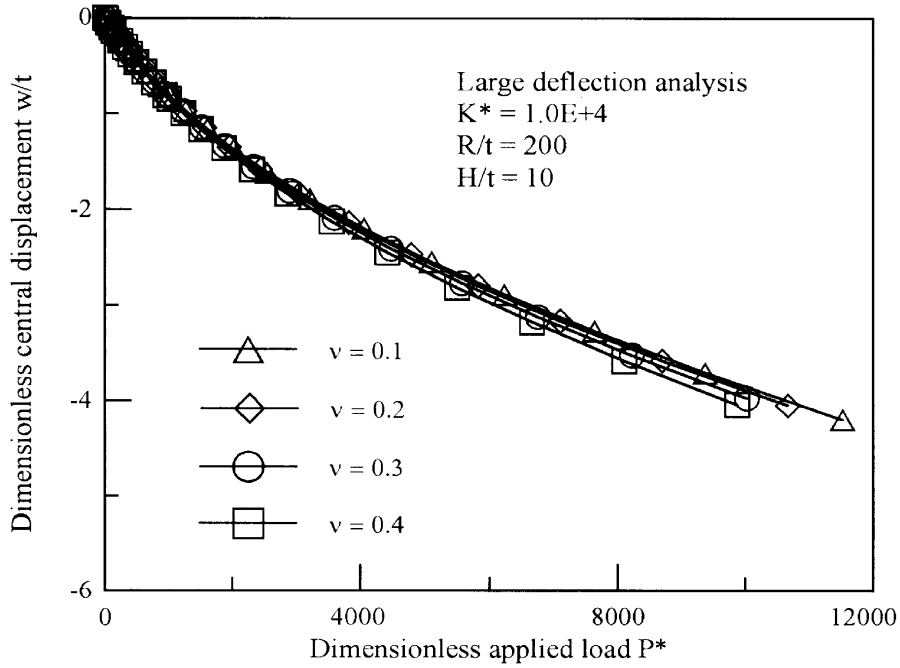

Fig. 8. Effect of Poisson's ratio for inverted spherical caps.

applications, inverted spherical caps are often used as shallow shell foundations for tower-shaped structures.

The results are presented in a dimensionless manner so that they are independent of the elastic modulus E and are only slightly dependent on the Poisson's ratio v. The results presented here are for a Poisson's ratio of 0.2, but the use of a Poisson's ratio of another value leads to only slightly different results (Fig. 8). The dimensionless load is given by $P^* = PR^2/(Dt)$, where P is the applied load, and D is the usual bending rigidity, and the dimensionless foundation stiffness parameter is given by $K^* = kR^4/D$ where k is the foundation stiffness. It may be noted that the dimensionless foundation stiffness defined here reduces to that used by Khathlan (1994) for circular plates.

5.2. *Effect of radius-to-thickness ratio on load deflection curves*

Figure 9 shows load deflection responses for inverted spherical caps with different values of the radius-to-thickness ratio R/t. The shells all have a depth of $H/t = 10$ and rest on a tensionless foundation with a foundation stiffness $K^* = 10^4$. It is clear that the dimensionless load deflection responses are independent of the R/t ratio unless R/t becomes so small ($R/t = 50$) that the shell is no longer shallow. The effect of the R/t ratio thus needs no further examination as far as shallow shells are concerned. The load deflection curve from a corresponding linear analysis shows that the effect of large deflections is strengthening and becomes important when the central vertical displacement exceeds around half the plate thickness.

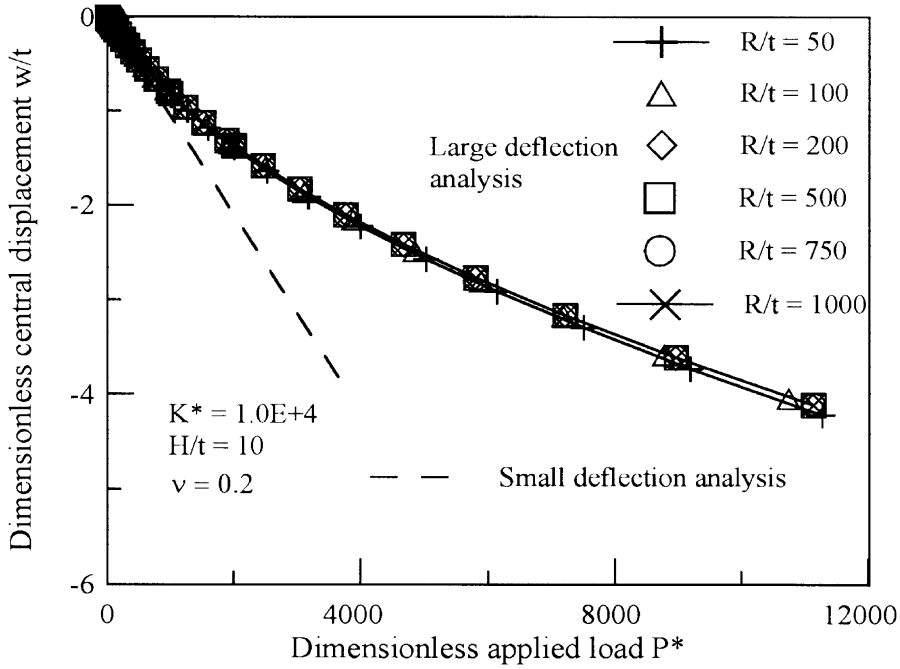

Fig. 9. Effect of radius-to-thickness ratio for inverted spherical caps.

5.3. Zones of contact and separation

Vertical deflections under different load levels of a spherical shell with $H/t = 10$ and $K^* = 10^4$ are shown in Fig. 10. Only results from the large deflection analysis are given. Although separation occurs around the middle between the centre and the edge of the shell, the upward deflections are very small compared with the downward deflections. The vast majority of the load applied on the shell is taken by the supporting medium under the central contact zone. Figure 11 shows the variation of the radial widths of the central contact zone (R_c/R) and the separation zone $[(R_s - R_c)/R]$ with the applied load. It is seen that as the load increases, the central zone of contact expands and the separation zone shrinks until separation completely disappears at a dimensionless load of around 350.

It should be noted that results from the small deflection analysis indicate that the zones of contact and separation do not depend on load levels (Fig. 11), as was noticed for circular plates. Therefore, a single chart (Fig. 12) can be developed from numerical results for the contact radius of the central contact zone for shells of different depths H/t. As long as deflections are below half the shell thickness, this chart can be used to determine the contact area of the shell with the supporting medium easily. It should be noted that for $H/t = 5$, 10 and 20, there is a sudden jump in the variation of the contact radius R_c/R with the dimensionless foundation stiffness K^*. For example, when $H/t = 5$, the contact radius R_c/R changes from around $R_c/R = 0.54$ to 1 (full contact) for a value of K^* around 3500. The finite element results plotted in Fig. 12 are only for cases where separation does occur. This chart provides useful information in a compact form for

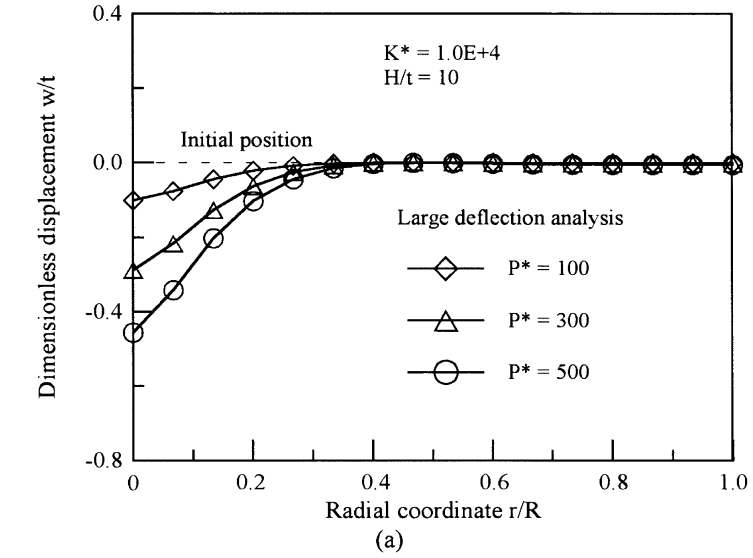

(a)

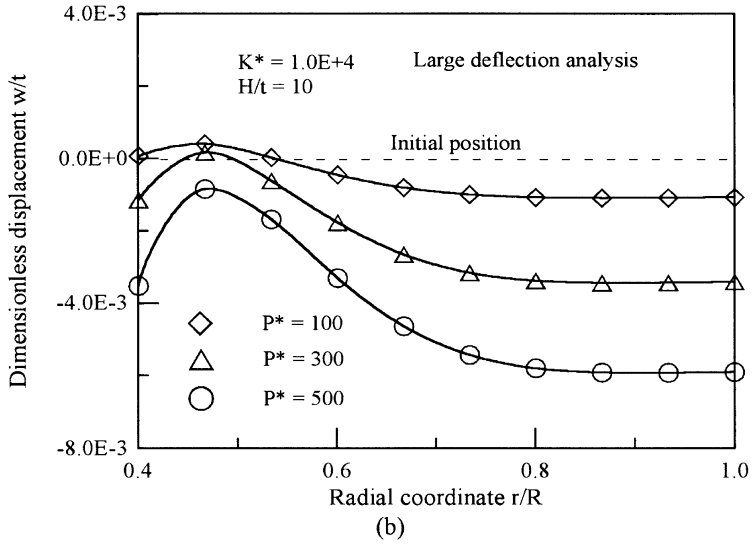

(b)

Fig. 10. Vertical deflections of an inverted spherical cap on tensionless foundation.

designers of shallow shells on a tensionless foundation supporting a concentrated load. Noting that the vertical reaction pressures are simply the vertical displacements in the central contact zone times the stiffness of the supporting medium, and the fact that the displacements vary almost linearly from the centre to the edge of the central contact zone, this chart may be used to estimate the soil pressures on a shallow shell foundation.

The above results on contact and separation zones for inverted spherical caps were obtained using a Poisson's ratio of 0.2 and R/t value of 200, but the results as presented in the dimensionless

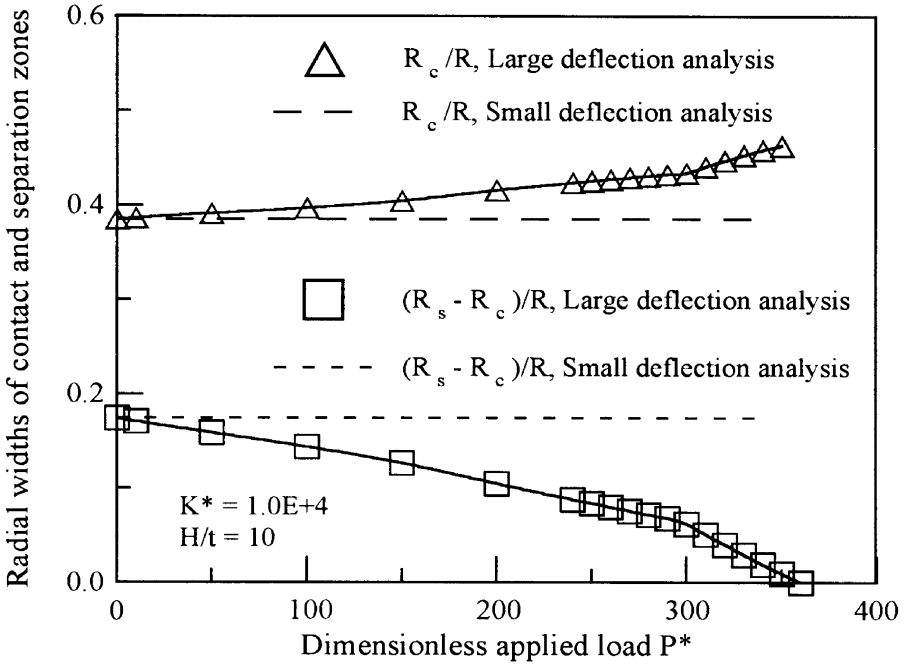

Fig. 11. Effect of load level on contact and separation zones of inverted spherical caps.

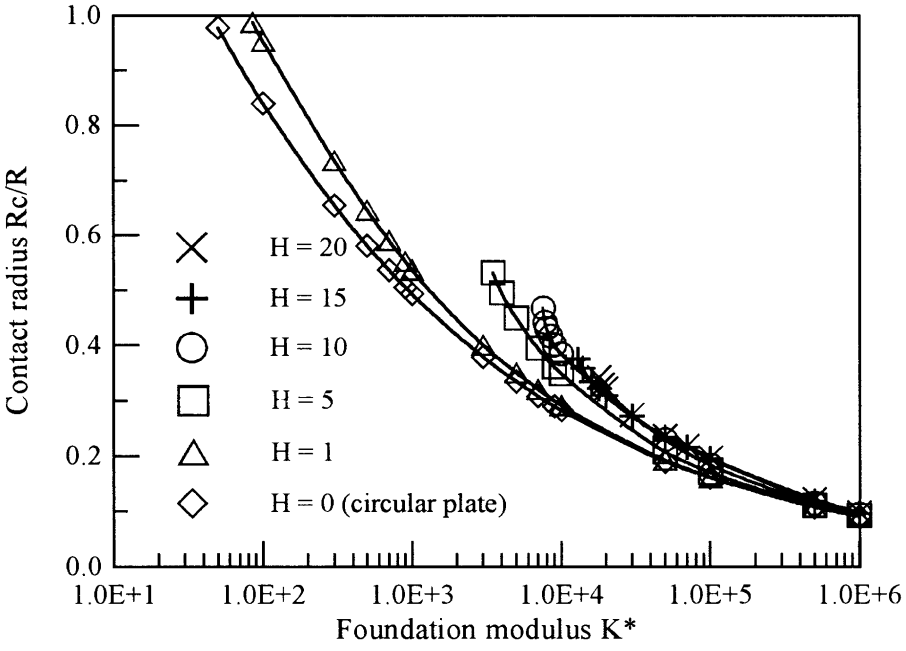

Fig. 12. Central contact radii from a small deflection analysis for inverted spherical caps.

Table 1
Effect of Poisson's ratio on contact radius of inverted spherical caps

R_c/R	$R/t = 50$	$R/t = 100$	$R/t = 200$	$R/t = 500$	$R/t = 750$	$R/t = 1000$
$v = 0.1$	0.3826	0.3856	0.3862	0.3863	0.3863	0.3863
$v = 0.2$	0.3814	0.3844	0.3850	0.3851	0.3851	0.3852
$v = 0.3$	0.3792	0.3825	0.3831	0.3833	0.3833	0.3833
$v = 0.4$	0.3760	0.3798	0.3804	0.3806	0.3806	0.3806

Table 2
Effect of Poisson's ratio on separation radius of inverted spherical caps

R_c/R	$R/t = 50$	$R/t = 100$	$R/t = 200$	$R/t = 500$	$R/t = 750$	$R/t = 1000$
$v = 0.1$	0.5624	0.5545	0.5524	0.5518	0.5517	0.5517
$v = 0.2$	0.5690	0.5611	0.5591	0.5585	0.5584	0.5584
$v = 0.3$	0.5805	0.5726	0.5707	0.5700	0.5700	0.5699
$v = 0.4$	0.5982	0.5903	0.5883	0.5877	0.5876	0.5876

manner have been taken to be valid for other values of R/t and Poisson's ratio as these two parameters have previously been shown to have little influence on the dimensionless results. Tables 1 and 2 confirm that similar to the situation for load-deflections curves, the effects of different R/t ratios and different values for the Poisson's ratio on the dimensionless contact and separation radii are small.

6. Spherical caps on tensionless foundations

6.1. General

Having examined the behaviour of inverted spherical caps, it was decided to consider the opposite case, dome type shallow spherical shells (referred to simply as spherical caps), to achieve a desirable degree of completeness of our knowledge on the interaction between shallow spherical shells and tensionless foundations. The geometry of spherical caps is defined by the same parameters as those used for inverted caps. The results are also presented in the same dimensionless manner for a Poisson's ratio of 0.2. Again, the use of a Poisson's ratio of another value leads to only slightly different results (Fig. 13).

6.2. Effect of radius-to-thickness ratio on load deflection curves

Figure 14 shows load deflection responses for spherical caps of different radius-to-thickness (R/t) ratios. These dimensionless plots confirm that they are independent of the R/t ratio. The

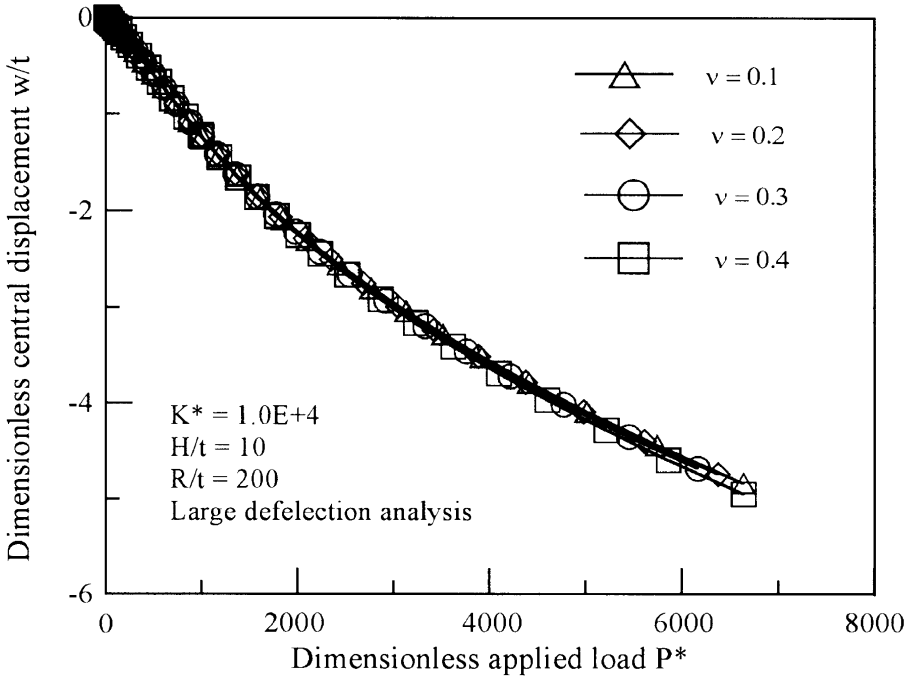

Fig. 13. Effect of Poisson's ratio for spherical caps.

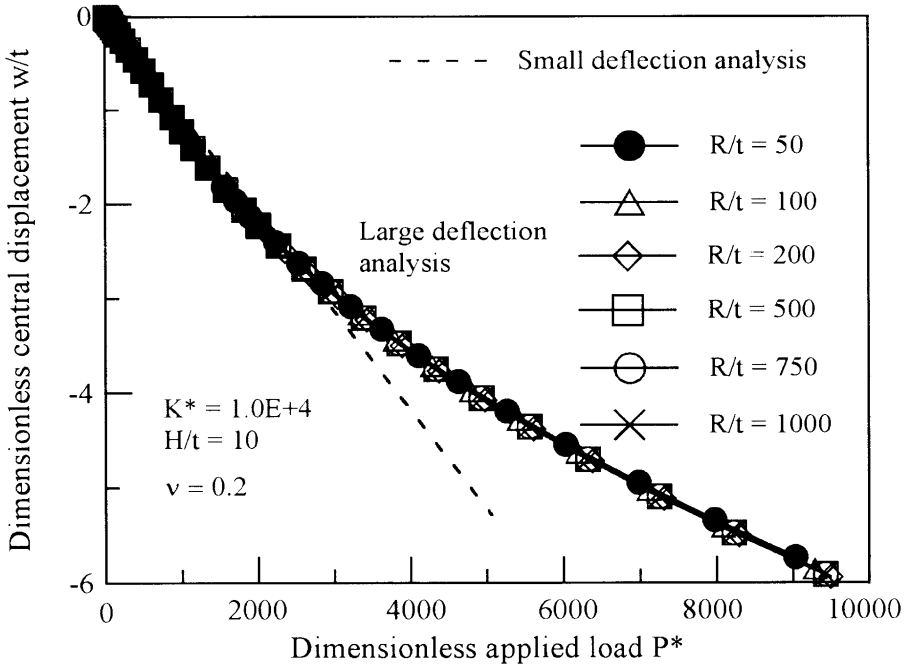

Fig. 14. Effect of radius-to-thickness ratio for spherical caps.

results here are found to be even less sensitive to R/t than those for inverted caps, as the deviation of the load-deflection curve for $R/t = 50$ from other cases is less than that for inverted caps. The effect of large deflections is initially weakening as the concentrated load leads to local high compression, but becomes strengthening when the deflections are large enough to deform the central part of the shell into an inverted cap.

6.3. Zones of contact and separation

The dimensionless results discussed here on contact and separation zones were again obtained assuming a Poisson's ratio of 0.2 and an R/t ratio of 200. The results are taken to be valid for other values of these two parameters as they have been shown to have little influence on these dimensionless results.

Vertical deflections under different load levels of a spherical shell with $H/t = 10$ and $K^* = 10^4$ are shown in Fig. 15. Only results from the large deflection analysis are given. Again separation initially occurs around the middle between the centre and the edge of the shell and the upward deflections are very small compared with the downward deflections. The behaviour of contact and separation zones under increasing loads of these caps is significantly different from that of inverted caps. For these caps, the central contact radius changes slightly at low loading and then shows little variation with load, so full contact can never be achieved (Fig. 16). On the other hand, the zone of separation grows with loading until the whole shell outside the central contact area loses contact with the foundation (Fig. 15).

The small deflection theory again predicts no changes in the contact and separation zone sizes as the load increases. A chart of the central contact radii based on the small deflection theory was developed, but it was found to be almost indistinguishable from the chart shown in Fig. 12 for inverted caps. Therefore, Fig. 12 can be used for both types of caps to determine the central contact zones at small deflections.

7. Nonlinear tensionless foundation

All the above results are for structures on linear tensionless foundations. To demonstrate the capability of the present analysis in dealing with nonlinear tensionless foundations, and to produce numerical results which may be useful for benchmarking purposes in the future, an inverted spherical cap (Fig. 6) with a Poisson's ratio of 0.2 and an R/t ratio of 200 on a nonlinear tensionless foundation was analyzed. The variation of the foundation reaction pressure normal to the shell surface with the normal displacement of the cap is given by

$$r = r_0(1 - e^{-\lambda w/t}) \tag{12}$$

r_0 is the limit pressure of the foundation, and λ is the dimensionless initial tangent stiffness of the nonlinear foundation [i.e. $\lambda = \partial(r/r_0)/\partial(w/t)$ at $w/t = 0$]. Such kind of foundation has been used by other researchers in modelling nonlinear soil behaviour (Calladine, 1996). The shell was analysed for two different foundations: (a) a nonlinear tensionless foundation with $\lambda = 5$ and $r_0/E = 1.805 \times 10^{-7}$ where E is the elastic modulus of the shell and (b) a linear tensionless foundation with a stiffness equal to the initial tangent stiffness of the nonlinear foundation. The shape

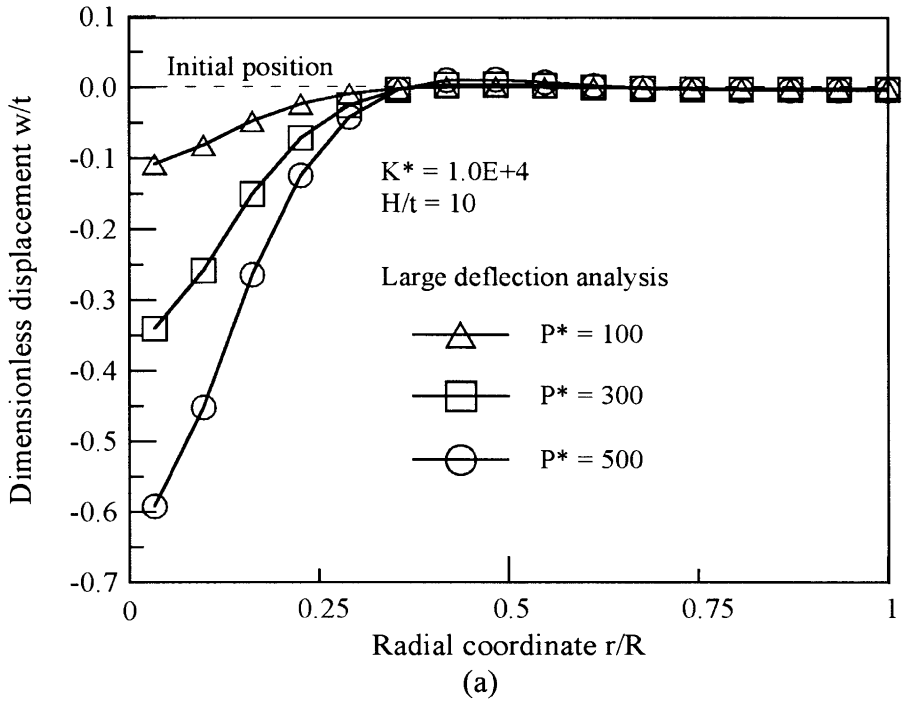

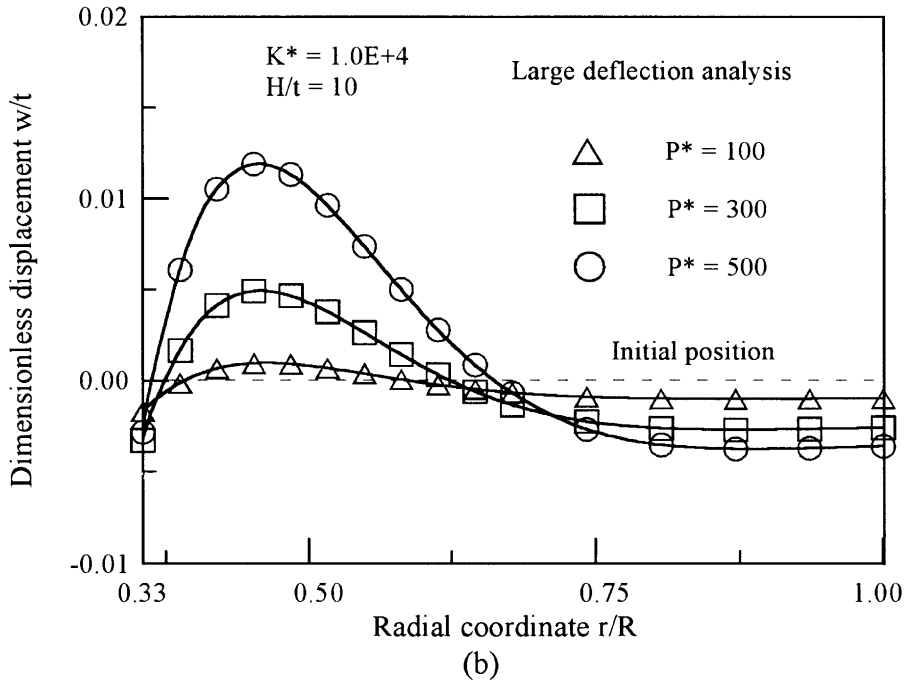

Fig. 15. Vertical deflections of a spherical cap on tensionless foundation.

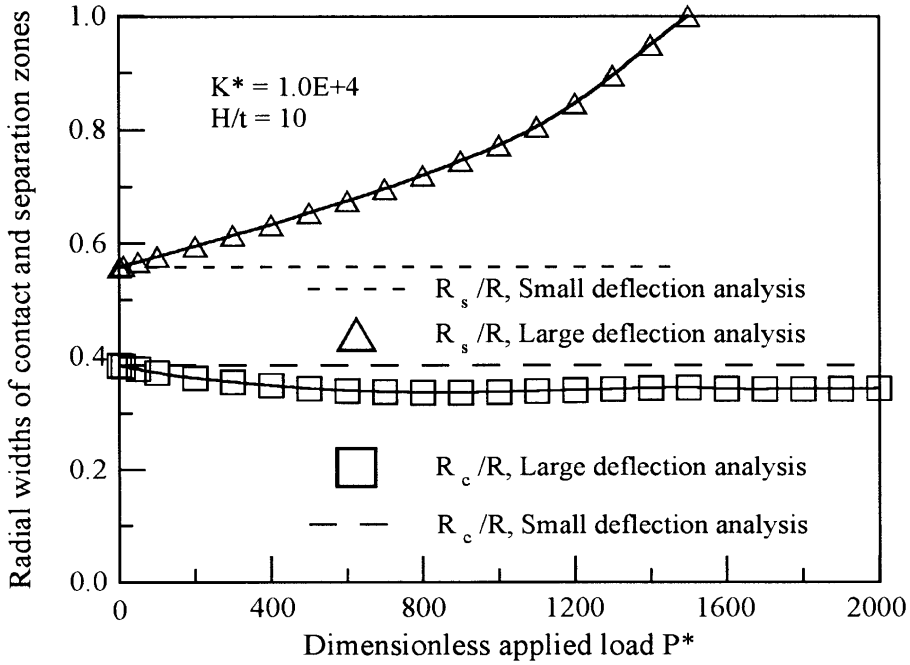

Fig. 16. Effect of load level on contact and separation zones of spherical caps.

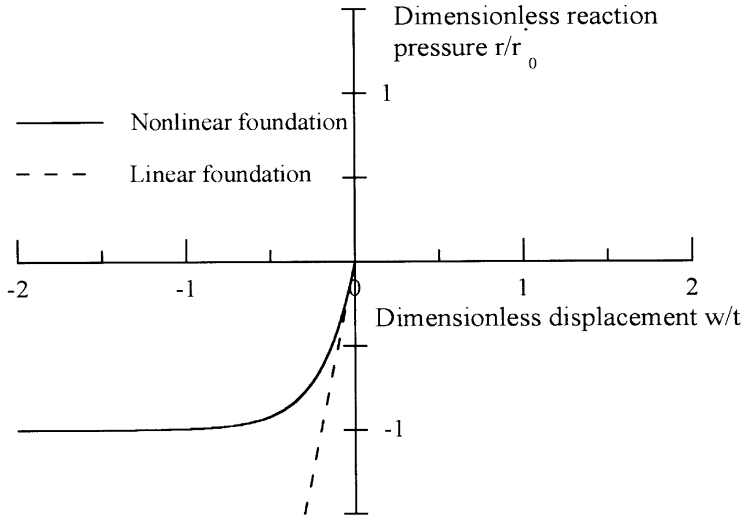

Fig. 17. Linear and nonlinear reaction pressure-displacement relationship.

of the reaction-normal displacement curve for the nonlinear foundation is shown in Fig. 17 together with that of the corresponding linear tensionless foundation. In the finite element analysis, the nonlinear foundation reaction-displacement curve was represented by a large number of discrete

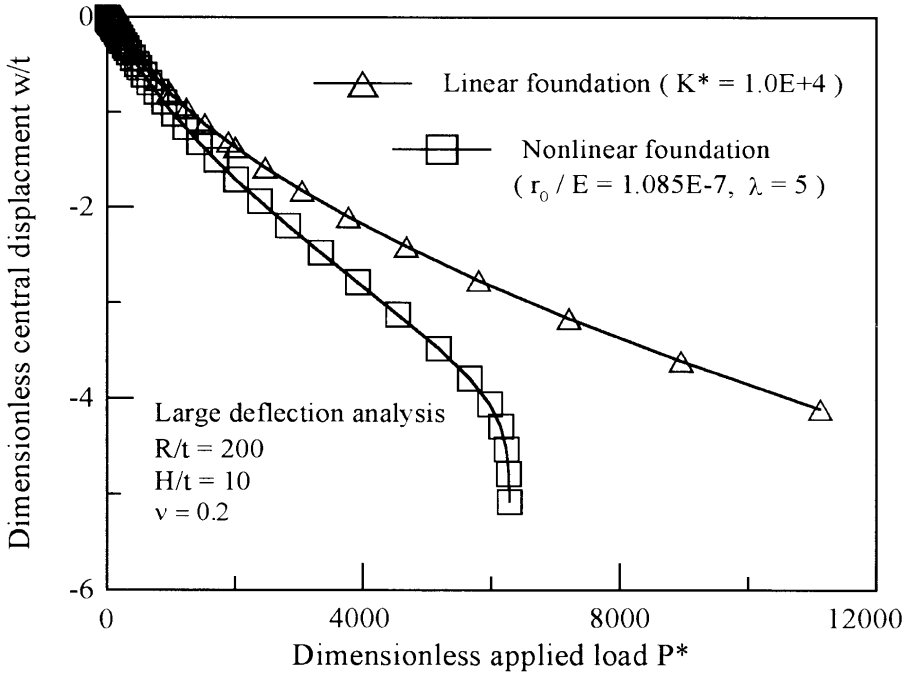

Fig. 18. Load-deflection curves of inverted spherical caps.

data points so that the curve could be very accurately modelled. Figure 18 shows the two load deflection responses. The effect of foundation nonlinearity is clearly demonstrated by comparing these two load deflection curves.

8. Conclusions

A finite element method for the large deflection analysis of axisymmetric shells and plates on a nonlinear tensionless elastic foundation has been presented, verified and then applied to investigate the behaviour of shallow spherical shells of both the dome type (i.e. spherical caps) and the inverted dome type (i.e. inverted spherical caps) subject to a central concentrated load on tensionless linear elastic foundations. An example of a shallow spherical shell on a nonlinear tensionless foundation has also been discussed. The following are the main conclusions:

(a) If the small deflection theory is used, then the contact area between a shallow spherical shell or a circular plate under a central concentrated load supported on a tensionless foundation is independent of load levels. A contact radius chart for shallow spherical shells under a central concentrated load has been developed. The chart provides useful information to designers of shallow shells on tensionless foundations.
(b) If the effect of geometric nonlinearity is included, the contact area changes with load levels. This effect for inverted spherical caps differs from that for spherical caps. For inverted spherical caps, the central contact area expands with loading, and full contact can be eventually achieved.

For spherical caps, the central contact area is relatively stable but the separation zone expands as the load increases. Consequently, shallow spherical shells of the inverted dome type is more appropriate as shell foundations since the contact area expands as load increases.

(c) The only existing results for the small deflection behaviour of shallow spherical shells on tensionless foundations have been found to be in error. The new results presented here are believed to be the first correct results for small and large deflection behaviour of shells on tensionless foundations. These results should be useful in benchmarking results form other sources in the future.

Acknowledgements

This research was supported by a research grant from the Hong Kong Polytechnic University, for which the authors are most grateful.

References

Calladine, C.R., 1996. Upheaval and lateral buckling of submarine pipelines. In: Chan, S.L., Teng, J.G., (Eds), Advances in Steel Structures. Elsevier Science, pp. 647–656.

Celep, Z., 1988a. Circular plates on tensionless Winkler foundation. ASCE J. Eng. Mech. Div. 114, 1723–1739.

Celep, Z., 1988b. Rectangular plates resting on tensionless elastic foundation. ASCE J. Eng. Mech. Div. 114, 2083–2092.

Ghosh, S.K., Paliwal, D.N., 1993. Analysis of a shallow spherical shell on no-tension foundation. Int. J. Pres. Ves. and Piping 56, 299–317.

Gladwell, G.M.L., 1976. On some unbonded contact problems in plane elasticity theory. ASME J. Applied Mechanics 43, 263–267.

Kamiya, N., 1977. Circular plates resting on biomodulus and no-tension foundations. ASCE J. Eng. Mech. Div. 103, 1161–1164.

Khathlan, A.A., 1994. Large-deformation analysis of plates on unilateral elastic foundation. ASCE J. Eng. Mech. Div. 120, 1820–1827.

Lewandowski, R., Switka, R., 1991. Unilateral plate contact with the elastic-plastic Winkler-type foundations. Computers and Structures 39, 641–651.

Li, H., Dempsey, J.P., 1988. Unbonded contact of a square plate on an elastic half-space or a Winkler foundation. ASME J. Appl. Mech. 55, 430–436.

Lin, L., Adams, G.G., 1987. Beam on tensionless elastic foundation. ASCE J. Eng. Mech. Div. 113, 542–553.

Luo, Y.F., Teng, J.G., 1998. Stability analysis of shells of revolution on nonlinear elastic foundations. Computers and Structures, 69, 499–511.

Rotter, J.M., Jumikis, P.T., 1988. Nonlinear strain-displacement relations for thin shells of revolution. Res. Rep. R563, School of Civil and Mining Engineering, University of Sydney.

Sokol-Supel, J., 1989. Elastoplastic circular plates resting unilaterally on elastic subgrade. Mech. Struct. and Machines 16, 335–357.

Svec, O.J., 1974. The unbonded contact problem of a plate on the elastic half space. Comput. Meth. Appl. Mech. Eng. 3, 105–113.

Teng, J.G., Rotter, J.M., 1989a. Elastic-plastic large deflection analysis of axisymmetric shells. Comput. and Struct. 31, 211–235.

Teng, J.G., Rotter, J.M., 1989b. Non-symmetric bifurcation of geometrically non-linear elastic-plastic axisymmetric shells subject to combined loads including torsion. Comput. and Struct. 32, 453–477.

Teng, J.G., Hong, T., 1997. Nonlinear thin shell theories for numerical buckling predictions. Thin-Walled Structures, accepted for publication.

Teng, J.G., Luo, Y.F., 1997. Post-collapse bifurcation analysis of shells of revolution by the accumulated arc-length method. Int. J. Num. Meth. Eng. 40, 2369–2383.

Tsai, N.C., Westmann, R.E., 1967. Beams on tensionless foundation. ASCE J. Eng. Mech. Div. 93, 1–12.

Vlasov, V.Z., Leontev, N.N., 1960. Beams, Plates and Shells on Elastic Foundations, Gosudarstvennoie Izdatel'stvo Fiziko-Matematicheskoj Literaturi. Moscow (in Russian); English Translation NASA TT-f-357, 1966.

Villaggio, P., 1983. A free boundary value problem in plate theory. ASME J. Appl. Mech. 50, 297–302.

Weitsman, Y., 1970. On foundations that react in compression only. ASME J. Appl. Mech. 37, 1019–1030.

Weitsman, Y., 1972. A tensionless contact between a beam and an elastic half-space. Int. J. Eng. Science 10, 73–81.

Winkler, E., 1867. Die Lehre von der Elastizitat und Festigkeit. Verlag H. Dominikus, Prague, Czechoslovakia.